Desalination and Water Treatment
www.deswater.com
doi: 10.1080/19443994.2016.1183232

57 (2016) 28436–28449
December

Taylor & Francis
Taylor & Francis Group

Adsorption of ciprofloxacin from aqueous solutions onto cationic and anionic flax noil cellulose

Dongying Hu, Lijuan Wang*

Key Laboratory of Bio-based Material Science and Technology of Ministry of Education, Northeast Forestry University, 26 Hexing Road, Harbin 150040, P.R. China, Tel./Fax: +86 451 82191693; emails: 465257973@qq.com (D. Hu), donglinwlj@163.com (L. Wang)

Received 11 December 2015; Accepted 22 April 2016

ABSTRACT

Cationic and anionic forms of cellulose were synthesized by introducing quaternary ammonium groups and carboxyl groups, respectively, to the skeleton of cellulose from flax noil. Batch adsorption experiments were carried out to explore the removal of ciprofloxacin (CIP) from aqueous solution using the cationic and anionic cellulose (cationic flax noil cellulose (CCFN) and anionic flax noil cellulose (ACFN)) obtained as adsorbents. The adsorbents were characterized by FTIR spectroscopy, X-ray photoelectron spectroscopy (XPS), XRD measurements, and SEM. The effects of various parameters including adsorbent dose, contact time, pH, and temperature on the adsorption performance were investigated. The adsorption data were analyzed using non-linear kinetics and isotherms models. FTIR, XPS, and XRD studies confirmed that the cationic and anionic groups had been successfully bound to the cellulose molecules after functionalization. SEM images showed that the surface morphology changed substantially after modification. Adsorption was dependent on solution pH, suggesting an electrostatic interaction mechanism. Under identical conditions, the adsorption capacity of CCFN for CIP was higher than that of ACFN. Adsorption of CIP onto CCFN was endothermic whereas adsorption onto ACFN was an exothermic process. The adsorption behavior of CIP on both adsorbents closely fitted a pseudo-second-order kinetic model, an intra-particle diffusion model, and the Langmuir isotherm. A thermodynamic analysis showed that adsorption was spontaneous and favorable.

Keywords: Adsorption; Ciprofloxacin; Kinetics; Isotherms; Modified flax noil

1. Introduction

Antibiotics are a group of substances that can effectively inhibit the growth of pathogens or other active materials [1]. At present, a large number of antibiotics are used not only to treat human and animal diseases but also widely in poultry feeding and aquaculture. Antibiotics play a very important role in disease prevention and growth promotion. Fluoroquinolones have been the antibiotics mostly applied to human therapy and veterinary treatment [2]. However, extensive use of antibiotics has resulted in their frequent detection in the final effluents of wastewater treatment plants (WWTPs). Many commonly used antibiotics do not biodegrade readily and consequently persist in the environment. The presence of antibiotics has been associated with a variety of

*Corresponding author.

adverse effects, including acute and chronic toxicity, micro-organism resistance, or effects on human health of endocrine-disrupting chemicals [3]. Moreover, these residues could threaten surface water quality and even that of groundwater as a result of leaching from agricultural fields [4].

Ciprofloxacin (CIP) is a zwitterionic antibiotic categorized as a second-generation fluoroquinolone of high use, which can effectively act against a wide range of gram-negative and gram-positive bacteria [5]. In addition, as the increasing of its use, large quantities of effluents containing CIP have been discharged into the environment. The excessive existence of CIP in the aquatic environment can lead to increased antibiotic resistance among bacteria and deleterious effects on water quality [6]. The emergence of resistance in bacteria can result from a direct one-step selection of resistant clones at the site of infection or an indirect two-step process in which antibiotic-resistant commensal bacteria are first selected in the natural ecosystems of humans [7]. Therefore, the removal of CIP from water has become an increasingly important and necessary task.

Several conventional methods, including adsorption, electrochemical removal, photolytic and photocatalytic treatments, oxidation, ozonation and peroxone processes, and biological treatment have been investigated [8,9]. Adsorption is an efficient treatment method for the removal of antibiotics from pharmaceutical wastewater. Activated carbon, with its large surface area and well-developed porous structure, has been widely used to remove organic and inorganic pollutants from aqueous solution. However, due to economic consideration, the use of activated carbon for wastewater treatment is often restricted. Recently, many other non-biomaterials have been used for the purification of pharmaceutical wastewater, such as montmorillonite [10], kaolinite [11], goethite [12], and magnetite [13]. However, there have been few studies on the use of biomass materials as adsorbents to remove antibiotics from pharmaceutical wastewater.

Cellulose, a low-cost, widely resourced, non-toxic, biodegradable, and renewable raw biomaterial, also can be chemically modified through reactions of the active hydroxyl groups on the glucose units [14]. Flax noil (FN) is the main byproduct of flax fiber separation by hackling. FN is a natural and sustainable biomaterial and its main component is cellulose [15]. Thus far, the use of FN as an adsorbent for purifying sewage has not been studied. To utilize FN as an adsorbent, further separation and chemical modification are necessary.

The objective of this study was to investigate the adsorption behavior of CIP on two different bioadsorbents. Cationic and anionic forms of FN were assembled using N,N-dimethyl-1-dodecylamine and citric acid as modifying agents. FTIR spectroscopy, X-ray photoelectron spectroscopy (XPS), XRD measurements, and SEM were used to characterize the adsorbents. The effects of various parameters, including the adsorbent dose, contact time, pH, and temperature, on the adsorption performance were studied. The kinetics, isotherms, and thermodynamics were also investigated in detail.

2. Experimental

2.1. Materials

Epichlorohydrin and citric acid (CA) were purchased from Kemiou Chemical Reagent Co., Ltd (Tianjin, China). N,N-Dimethyl-1-dodecylamine ($C_{14}H_{31}N$; 98% pure; $M_W = 213.4$) was obtained from Heowns Chemical Reagent Co., Ltd (Tianjin, China). CIP Hydrochloride Monohydrate (CIP, $C_{17}H_{18}FN_3O_3 \cdot HCl \cdot H_2O$, $M_W = 367.80$) with a purity higher than 98.0% was purchased from Tokyo Chemical Industry Co., Ltd (TCI China). Its molecular structure is shown in Fig. 1. All other chemicals and reagents were of analytical grade and without further purification.

2.2. Adsorbents preparation

2.2.1. Separation and purification of FN

FN obtained from Harbin Linen Textile Co., Ltd (Harbin, China) was used as a raw material for adsorbent preparation. The FN was washed several times with tap water to remove dust and other impurities and then air-dried. Cellulose was separated through alkali pretreatment method, as reported in previous study [16]. Then, the obtained cellulose was bleached to remove the residual lignin according to the previous method [17]. Finally, the dry cellulose was ground into small particles with a size of 80–120 mesh for further modified process (CFN).

2.2.2. Preparation of cationic flax noil cellulose

Ten grams of CFN powder and 250 mL of 20 wt% NaOH solution was added into the three-neck round bottom flask and stirred at room temperature for 2 h to obtain the activated cellulose. Then the solution was removed and 250 mL of 10 wt% NaOH solution and 240 mL of epoxy chloropropane were added. The mixture was heated to 65°C in a water bath and stirred for 6 h. Then the solution was removed by filtering, and 40 v/v % of N,N-Dimethyl-1-dodecylamine

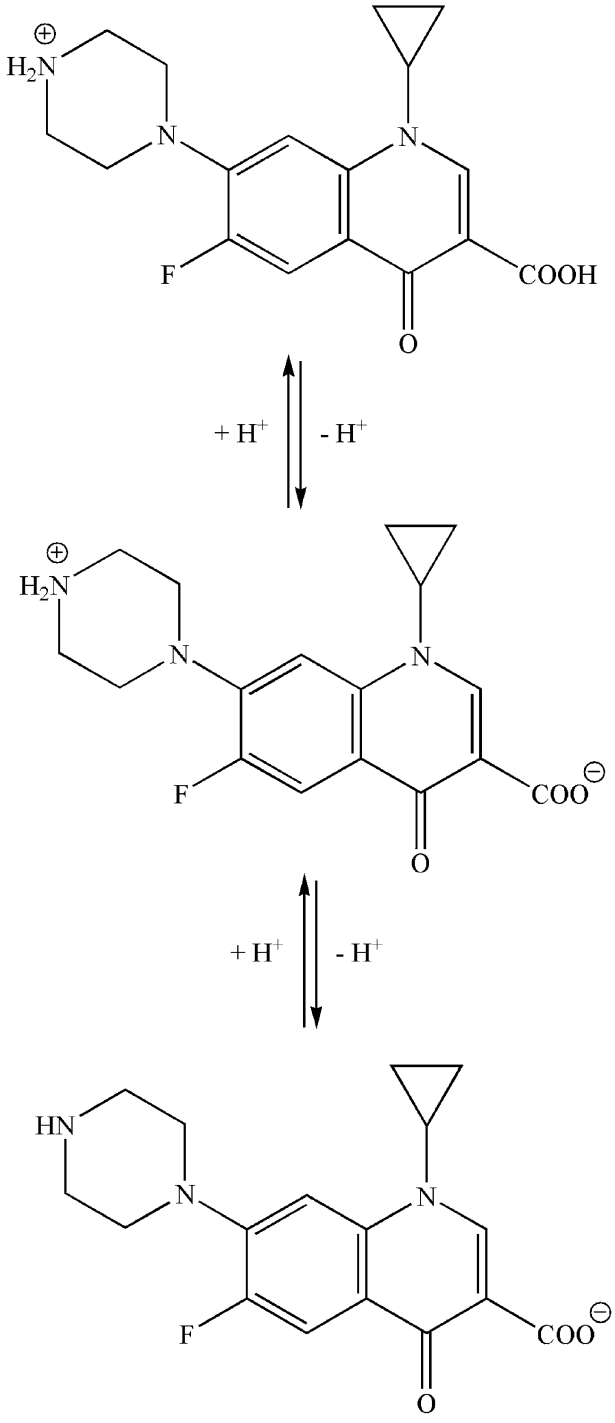

Fig. 1. The molecular structure of CIP.

in isopropanol (100 mL) was added to the residue and the mixture was heated to 80°C agitated for 3 h. The product was filtered and washed with anhydrous ethanol to remove the residential N,N-Dimethyl-1-dodecylamine, followed by 0.1 M NaOH, 0.1 M HCl to adjust the solution pH around 7, and then by a plenty of distilled water. The cationic flax noil cellulose (CCFN) was dried in an oven at 60°C for 12 h. Synthetic reaction for the CCFN is shown in Fig. 2.

2.2.3. Preparation of anionic flax noil cellulose

CFN powder (20 g) and 200 mL of 0.8 mol/L citric acid solution were added to a reaction vessel and stirred for 30 min; then the mixture was ventilated with drying at 50°C for 24 h and was next heated up to 120°C for 120 min to accomplish esterification. After cooling, the mixture was washed with distilled water to remove the residual citric acid. Then the solution was removed by filtering, and 0.1 mol/L NaOH solution (200 mL) was added to the residue and the mixture was stirred for 60 min. Finally, the product (anionic flax noil cellulose (ACFN)) was washed with distilled water to neutral pH and dried in an oven at 60°C for 12 h. Synthetic reaction for the ACFN is shown in Fig. 3.

2.3. Adsorbents characterization

FTIR spectra of the samples were obtained on a Nicolet 6700 spectrometer (Thermo Fisher Scientific Co., Ltd, MA, USA). Measurements were done in attenuated total reflection mode at a resolution of 4 cm^{-1}. The XPS experiments were performed with a K-Alpha XPS analyzer (Thermo Fisher Scientific Company, USA). The nitrogen content (N %) was measured on an element analyzer (EA 3000, Arvator, Italy). XRD patterns of the samples were obtained using a D/max-2200 diffractometer (Cu-K_α target, 40 kV, 30 mA) operated at 1,200 W (Rigaku, Japan). The morphology of the samples was observed after coated with a gold layer under a Quanta 200 scanning electron microscope (Philips-FEI Co., Ltd. The Netherlands). The Brunauer–Emmett–Teller (BET) pore structure parameters of samples were measured using a JW-BK132F instrument (JWGB Sci. & Tech. Co., Ltd, Beijing, China). Zeta potentials of adsorbents at different pH solution were measured using a zetasizer nano ZEN3600 equipment (Malvern instrument company, UK), the measurements were repeated at least three times. The points of zero charge (pH_{pzc}) of CCFN and ACFN were measured by means of the previous method.

2.4. Batch adsorption studies

Batch adsorption experiments were performed to determine the ability of adsorbents to remove CIP

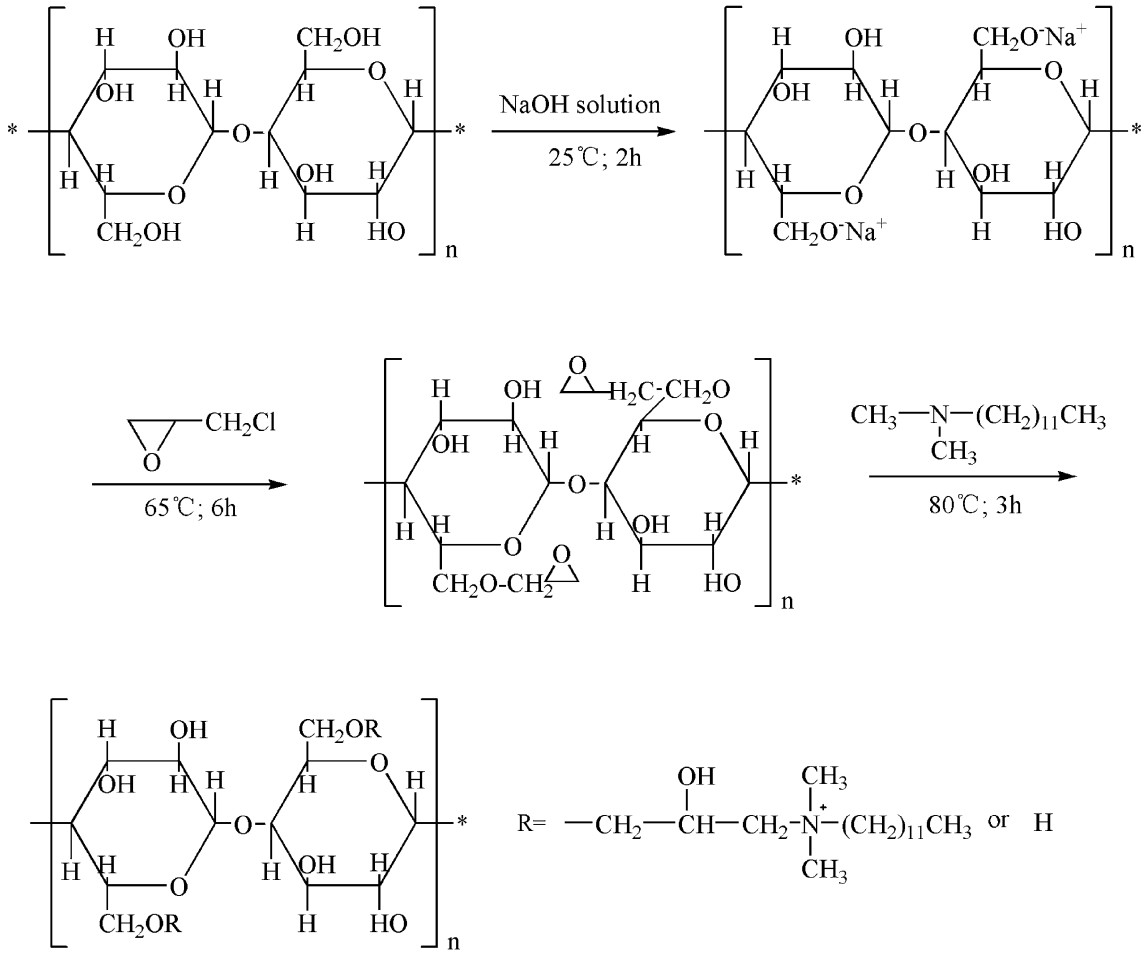

Fig. 2. Synthetic reaction for the CCFN.

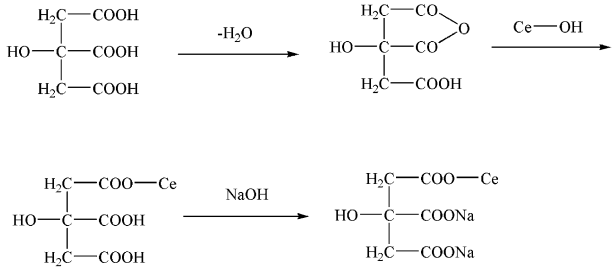

Fig. 3. Synthetic reaction for the ACFN.

from aqueous solutions in a water bath oscillator. In each adsorption experiment, a certain amount of adsorbent and 50 mL of CIP solution were added into a 250 mL conical flask shaken at 120 rpm. The influences of adsorbent dose, contact time, and temperature on the adsorption performances were investigated. The effects of pH on the adsorption of CIP by CCFN and ACFN were also determined. The pH values were adjusted in the range from 3 to 10 by adding a few drops of NaOH or HCl solution. After adsorption, the adsorbents were separated from aqueous solution using a centrifuge at 4,000 rpm for 10 min. The residual CIP concentrations were measured by an ultraviolet–visible (UV–vis) spectrophotometer (UV-2600, Shimadzu, Kyoto, Japan) at λ_{max} = 275 nm. Each batch experiments were repeated three times. The removal efficiency (R, %), the adsorption capacities at equilibrium (q_e, mg/g), and at time t (q_t, mg/g) were calculated using the following equations:

$$R = (C_0 - C_t)/C_0 \times 100\% \quad (1)$$

$$q_e = (C_0 - C_e) \times V/M \quad (2)$$

$$q_t = (C_0 - C_t) \times V/M \quad (3)$$

where C_0, C_e, and C_t (mg/L) are the CIP concentration of the initial solution, the residual solution at equilibrium, and at time t, respectively. V is the volume of CIP solution and M is the mass of adsorbent.

2.5. Kinetics studies

In this study, nonlinear models of pseudo-first-order kinetic, pseudo-second-order kinetic, and Elovich were used in predicting the adsorption process of CIP onto CCFN and ACFN. The intra-particle diffusion model was also investigated. The kinetics of adsorption was determined by analyzing the CIP adsorbed from aqueous solution at various time intervals. The four kinetic models are given as follows [18]:

Pseudo-first-order kinetic model:

$$q_t = q_e(1 - e^{-k_1 t}) \tag{4}$$

Pseudo-second-order kinetic model:

$$q_t = k_2 q_e^2 t/(1 + k_2 q_e t) \tag{5}$$

Elovich model:

$$q_t = \ln(1 + \alpha\beta t)/\beta \tag{6}$$

The intra-particle diffusion model:

$$q_t = k_i t^{0.5} + C \tag{7}$$

where q_e and q_t (mg/g) are CIP adsorption capacity at equilibrium and time t (min). k_1 (1/min) and k_2 (g/(mg min)) are rate constants of pseudo-first-order and pseudo-second-order, respectively. α is the initial sorption rate (mg/(g min)) and β is the desorption constant (g/mg) of the Elovich model. k_i is the intra-particle diffusion rate constant (mg/(g $\text{min}^{0.5}$)) and C is a constant (mg/g).

The Arrhenius equation was used to calculate the activation energy of the adsorption:

$$\ln k_2 = -E_a/RT + \ln k_0 \tag{8}$$

where E_a (kJ/mol) is the activation energy of the adsorption. k_2 (g/(mg min)) is the rate of constant of the pseudo-second-model. R is the gas constant (8.314 J/(mol K)). T (K) is the absolute temperature. The value of E_a is evaluated by plotting $\ln k_2$ vs. $1/T$.

2.6. Isotherms studies

In this study, four adsorption isotherms were used to fit the adsorption of CIP onto the two different cellulose types of CCFN and ACFN. The non-linear fitting models were presented as follows [19]:

The Langmuir model:

$$q_e = q_m K_a C_e/(1 + K_a C_e) \tag{9}$$

$$R_L = 1/(1 + K_a C_0) \tag{10}$$

The Freundlich model:

$$q_e = k_F C_e^{1/n_F} \tag{11}$$

The Temkin model:

$$q_e = B \ln A_T C_e, \quad B = RT/b_T \tag{12}$$

Sips model:

$$q_e = q_m K_s C_e^{1/n}/(1 + K_s C_e^{1/n}) \tag{13}$$

where q_m (mg/g) is the maximum adsorption capacity, K_a (L/mg) is the Langmuir adsorption constant. The value of R_L indicates whether the adsorption behavior is favorable or unfavorable: unfavorable ($R_L > 1$), linear ($R_L = 1$), favorable ($0 < R_L < 1$), or irreversible ($R_L = 0$) [20]. k_F ($\text{mg}^{1-(1/n)}/(\text{g L}^{-1/n})$) is the Freundlich constant and n_F is the heterogeneity factor. B is the Temkin constant which is related to heat of adsorption, A_T (L/mg) is the equilibrium binding constant. K_s (L/mg) is the Sips constant and n is the Sips model exponent.

2.7. Thermodynamic studies

Thermodynamic parameters of CIP adsorption onto CCFN and ACFN including standard free energy change (ΔG°), standard enthalpy change (ΔH°), and standard entropy change (ΔS°) were determined by the following equations:

$$\Delta G^\circ = -RT \ln K_d \tag{14}$$

$$K_d = q_e/C_e \tag{15}$$

$$\ln K_d = -\Delta H^\circ/RT + \Delta S^\circ/R \tag{16}$$

where R is the universal gas constant (8.314 J/(K mol)), and K_d is the equilibrium constant for the adsorption at standard temperature and pressure. ΔH° and ΔS° were obtained from the slope and intercept of the linear plot of ln K_d vs. $1/T$.

2.8. Statistical analysis

Three parallel experiments were tested, and data were analyzed by the one-way analysis of variance (ANOVA) through the SPSS software and differences among mean values were processed by the Duncan's multiple-range tests. Significance was defined at p-values of <0.05.

3. Results and discussion

3.1. Characterization of adsorbents

FTIR spectra of CFN, CCFN, and ACFN are shown in Fig. 4(a). For CFN, the bands at 3,310 and 2,893 cm^{-1} are attributed to the O–H stretching vibration of the hydroxyl groups and the C–H stretching vibration of the $–CH_2–$ groups, respectively. A series of bands at 1,162, 1,108, 1,053, and 1,025 cm^{-1} correspond to –C–O–C– bonds in the anhydroglucose unit of the cellulose molecule [21]. The spectrum of CCFN shows characteristics similar to CFN except for some slight differences. After modification with quaternary ammonium groups, the O–H stretching vibration bands weakened, broadened, and shifted to 3,336 cm^{-1}; however, the intensity of the $–CH_2–$ group increased; moreover, a new peak at 1,454 cm^{-1} appeared and is attributed to C–N vibrations of $–N^+(C_2H_5)_3Cl^-$. All of these changes indicate that the quaternary ammonium group was successfully attached to the CFN skeleton. As shown in Fig. 4(b), the peaks at 401.70 eV in the XPS spectrum further proved that CCFN contains nitrogen in quaternary valence states [22].

In the ACFN spectrum, a decrease in intensity of the O–H peak indicated CA reacted with the hydroxyl groups on CFN [23]. Moreover, new peaks at ~1,731 and 1,581 cm^{-1} were attributed to the absorption vibrations of the ester groups and carboxylate groups, respectively [24]. All of these changes indicate that carboxylic anions were introduced into the CFN molecule after modification with citric acid.

Furthermore, the degrees of substitution of CCFN (N%: 2.03%) and ACFN (O%: 2.69%) obtained from elemental analyses were 0.42 and 0.45, and calculated according to the previous method [25], respectively, which further support the above results.

The XRD patterns of CFN, CCFN, and ACFN are shown in Fig. 4(c). The XRD pattern of CFN displays the typical cellulose I structure at $2\theta = 16.24^\circ$, 22.76°, and 34.67°. In the CCFN pattern, characteristic peaks disappeared and new peaks occurred at 20.24°. The crystalline structure of CFN had evidently changed, which indicates that the hydrogen bonds of the original CFN were broken during the modification process. The XRD pattern obtained for ACFN has characteristics that are similar to CFN except for the increased intensity, which indicates that the crystallinity of CFN was significantly affected by CA modification. This is because the CA molecule can penetrate the amorphous regions and produce crosslinks between the cellulose units, thus resulting in an increase in crystallinity [26].

The SEM images of CFN, CCFN, and ACFN are shown in Fig. 5. CFN has a structure similar to a bamboo joint. After modification, the surface morphology obviously changed and the bamboo joint structure disappeared. The surface of CCFN was coarse and rough. The prepared ACFN appeared to have a uniform

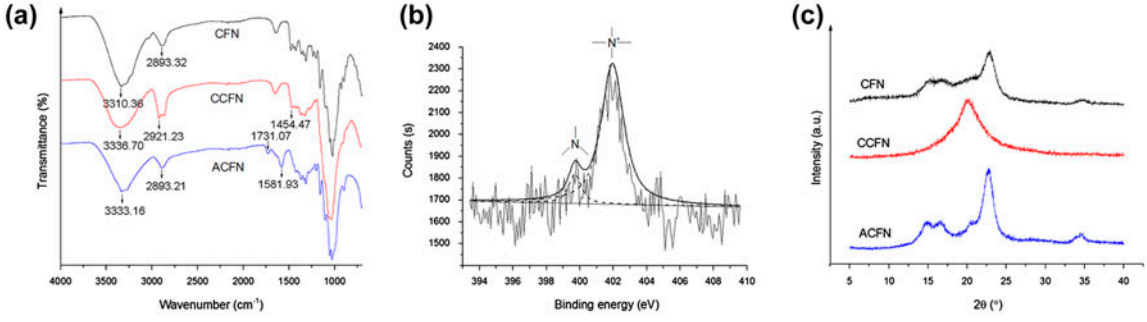

Fig. 4. (a) FTIR spectra of CFN, CCFN, and ACFN, (b) N 1s spectrum of CCFN and (c) XRD patterns of CFN, CCFN, and ACFN.

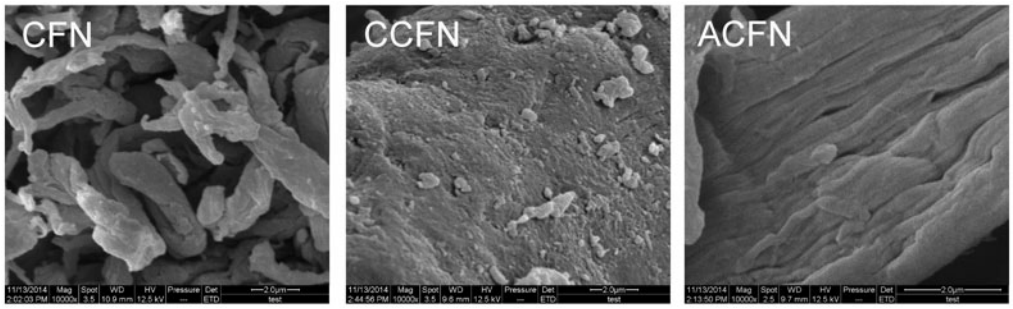

Fig. 5. SEM images of CFN, CCFN, and ACFN.

wrinkled structure. Moreover, the values of S_{BET} are 4.35 and 3.90 m^2/g for CCFN and ACFN, respectively. The values of pore size are 5.19 and 5.18 nm for CCFN and ACFN, respectively. These results are consistent with the SEM observations. Furthermore, the values of pore sizes are lower than that of CIP molecule size (29.97 nm) reported by Li et al. [27]. These BET pore structure parameters are not the key factor for CIP adsorption in this study.

3.2. Effects of solution pH

The effects of solution pH on CIP adsorption onto CCFN and ACFN were studied in the pH range of 3–10 (Fig. 6(a)). Adsorption capacity increased with increasing pH and reached a maximum value at pH 7 and decreased sharply with increasing pH above 7. CIP (pK_{a1} = 6.1, pK_{a2} = 8.7) exhibits pH-dependent speciation in its different forms as a cation (<6.1), zwitterion (6.1–8.7), and anion (>8.7) [28]. The pH_{pzc} values of CCFN and ACFN were 7.41 and 6.32, respectively (Fig. 6(b)). For CCFN, a higher positive charge developed on its surface at pH values below pH_{pzc}, and this positive charge decreased at pH values above pH_{pzc}. For ACFN, a lower negative charge developed on its surface at pH values below pH_{pzc}, and this negative charge increased at pH values above pH_{pzc}. The above results are in agreement with results from the zeta potential test (Fig. 6(c)). For CCFN, the possible adsorption mechanism for the adsorption of CIP is shown in Fig. 7. At pH < 6.1 there was

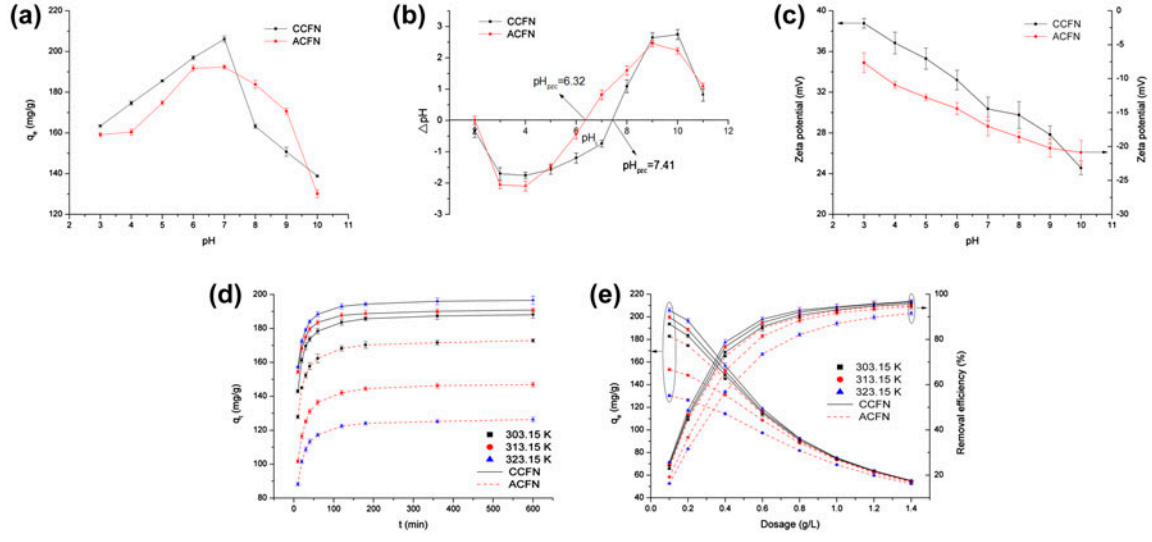

Fig. 6. (a) Influence of pH on the adsorption of CIP onto CCFN and ACFN (dosage = 0.4 g/L; t = 10 h; C = 80 mg/L; V = 50 mL), (b) point of zero charge of CCFN and ACFN, (c) zeta potential curves vs. pH of CCFN and ACFN, (d) influence of contact time on the adsorption of CIP onto CCFN and ACFN (dosage = 0.4 g/L; C = 80 mg/L; V = 50 mL; pH = initial pH), (e) influence of dosage on the adsorption of CIP onto CCFN and ACFN (C = 80 mg/L; V = 50 mL; pH = initial pH; t = 10 h).

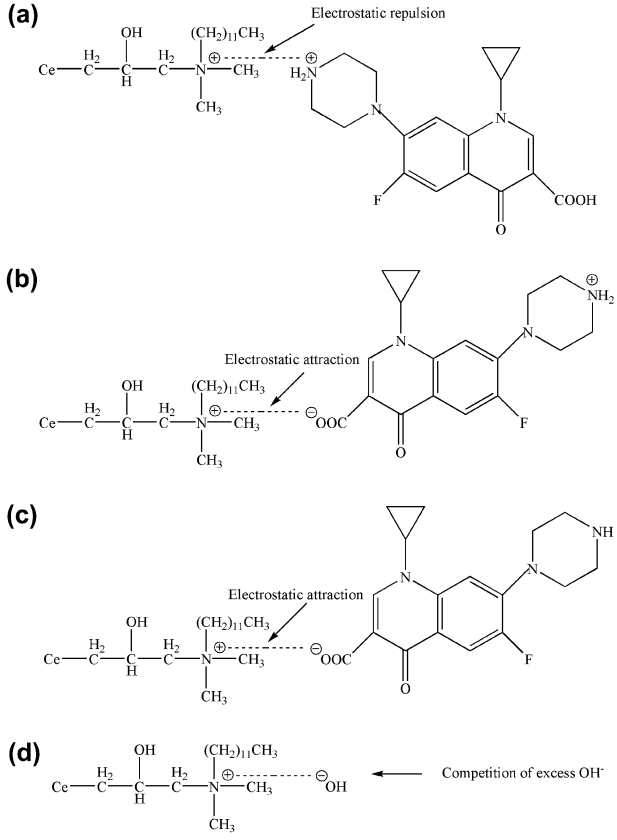

Fig. 7. The possible adsorption mechanism for the adsorption of CIP onto CCFN.

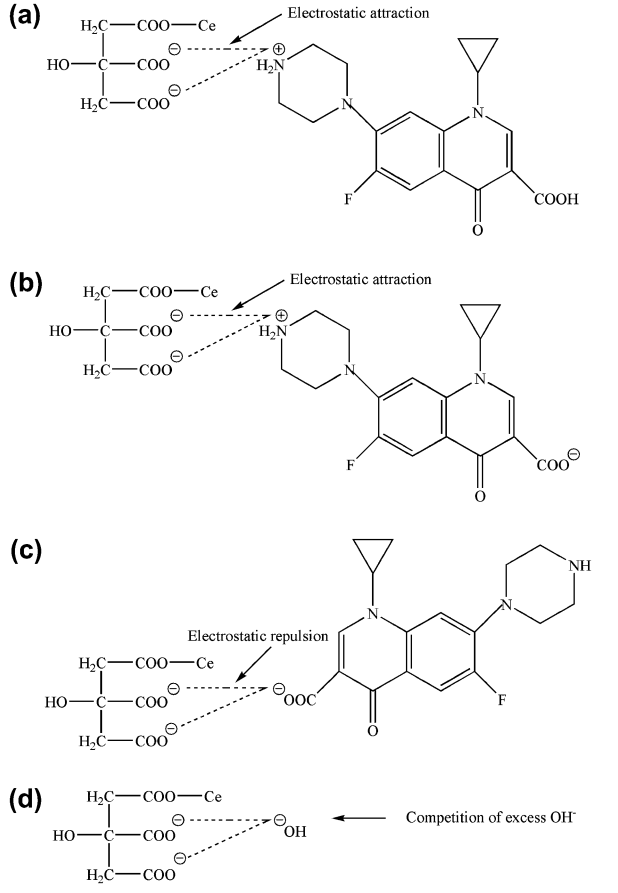

Fig. 8. The possible adsorption mechanism for the adsorption of CIP onto ACFN.

electrostatic repulsion between the $-NH_2^+$ groups of CIP and the quaternary amino groups of the CCFN, resulting in low adsorption capacity. Upon increasing the pH but keeping it still below 7.41, the numbers of $-NH_2^+$ groups decreased while the numbers of $-COO^-$ groups increased, thereby increasing the adsorption capacity. At higher pH values, competition from the OH^- ions played a major role and resulted in reducing the adsorption capacity. For ACFN, the possible adsorption mechanism for the adsorption of CIP is shown in Fig. 8. At lower pH values, some of the $-COO^-$ groups were transformed into –COOH groups, so that the low adsorption capacity was due to a decrease in the electrostatic attraction between the $-NH_2^+$ groups of CIP and the $-COO^-$ groups of the ACFN [29]. With increasing pH, the adsorption mechanism was mainly controlled by the electrostatic attraction, resulting in increasing adsorption capacity. However, under alkaline conditions, the numbers of $-NH_2^+$ groups decreased while the numbers of $-COO^-$ groups increased, thereby decreasing the electrostatic attraction and increasing the electrostatic repulsion. Moreover, competition from the OH^- ions also occurred during the adsorption process.

3.3. Effects of contact time

The effects of contact time on CIP adsorption onto CCFN as well as ACFN are shown in Fig. 6(d). The adsorption rate was rapid during the first 60 min; subsequently, it decreased gradually and reached equilibrium at 120 min, indicating that a shaking time of 10 h was sufficient for the other adsorption experiments. The high adsorption rate in the first stage may be due to a high driving force, which causes CIP molecules to transfer rapidly to the surface of the adsorbents, along with the availability of numerous active binding sites. The decrease in adsorption rate may be attributed to the reduced numbers of remaining active sites and the increasing numbers of long-range transformations onto the surface of adsorbent. It is obvious that the equilibrium adsorption capacity by CCFN was higher than that of ACFN.

3.4. Effects of adsorbent dose

The effects of CCFN and ACFN dosage on the removal efficiencies and adsorption capacities of CIP were investigated (Fig. 6(e)). Increasing the adsorbent dose resulted in greater removal efficiency (R) and a decrease in the adsorption capacity. The positive correlation between adsorbent dose and removal efficiency can be related to the number of available adsorption active sites, which increases by increasing the adsorbent dose [30]. The R values remained nearly constant above a dose of 0.1 g/L; this phenomenon is due to the non-availability of adsorption active sites and the establishment of equilibrium between adsorbent and adsorbate. The negative correlation between adsorbent dose and adsorption capacity can be attributed to the decrease in total surface area of the adsorbent available to CIP molecules resulting from overlapping or aggregation of adsorption sites [31].

3.5. Adsorption kinetics

The fitted curves and parameters for the three types of adsorption kinetics are presented in Fig. 9 and Table 1, respectively. The correlation coefficients of pseudo-second-order kinetics were higher than those of the other types of kinetics. Moreover, the calculated values of $q_{e,cal}$ were closer to the experimental data, indicating that the removal of CIP by CCFN and ACFN fitted pseudo-second-order kinetics best. Pseudo-second-order kinetics suggests that the adsorption process of CIP might be controlled by valence forces through the sharing or exchange of electrons between CIP and CCFN or ACFN [32]. The k_2 values of CCFN are higher than those of ACFN at the same temperature, indicating that the time required to reach an equilibrium state is shorter with CCFN than ACFN [33].

In order to investigate the potential rate-controlling steps, including diffusion and chemical or physical

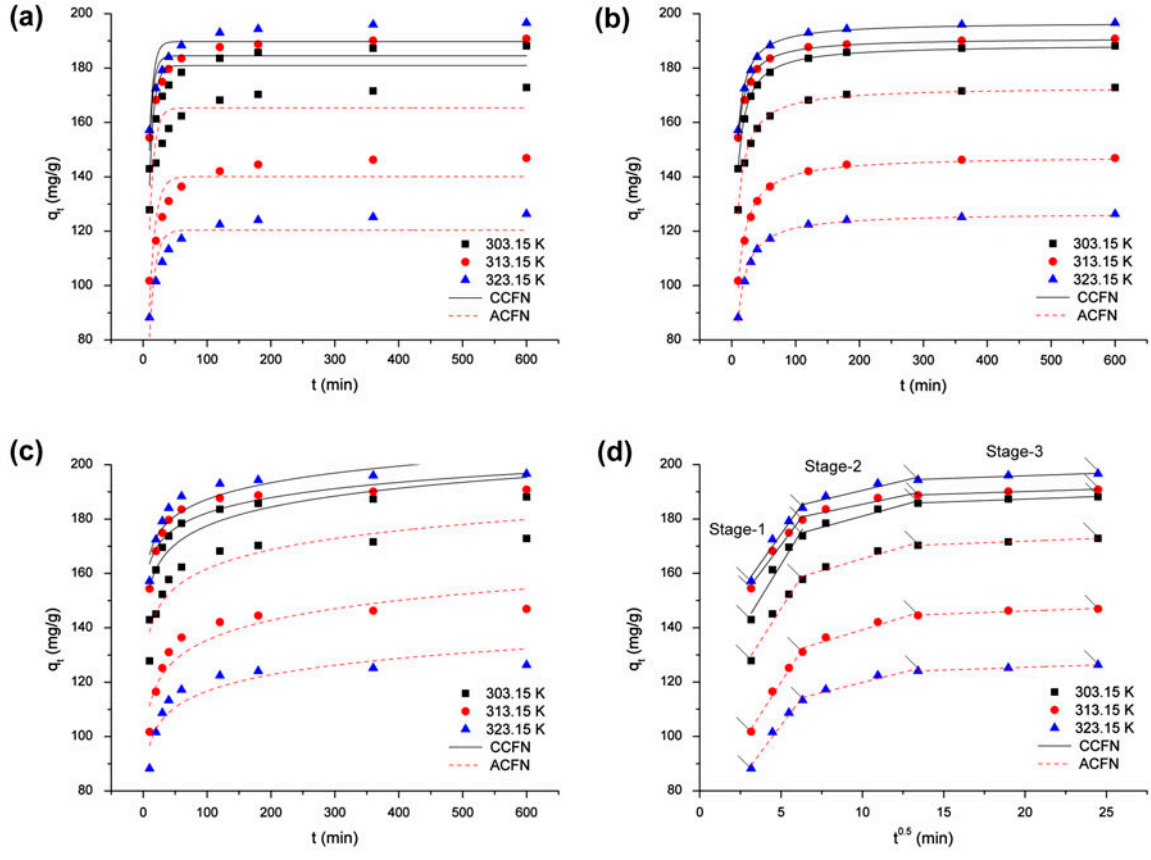

Fig. 9. Adsorption kinetics of CIP on CCFN and ACFN: (a) pseudo-first-order kinetic model, (b) pseudo-second-order kinetic model, (c) Elovich model and (d) intra-particle diffusion model.

Table 1
Kinetics parameters on the adsorption of CIP onto CCFN and ACFN

	CCFN			ACFN		
Kinetics	303.15 K	313.15 K	323.15 K	303.15 K	313.15 K	323.15 K
Pseudo-first-order						
k_1	0.061	0.072	0.070	0.057	0.047	0.049
$q_{e,cal}$	180.92	184.49	189.74	165.34	140.05	120.41
R^2	0.7644	0.7045	0.7074	0.7465	0.7599	0.7715
Pseudo-second-order						
k_2	0.016	0.019	0.021	0.017	0.016	0.014
$q_{e,cal}$	188.67	191.10	196.85	173.08	147.63	126.73
R^2	0.9982	0.9925	0.9929	0.9945	0.9904	0.9941
Elovich model						
α	56.87	84.06	144.80	90.25	60.43	40.95
β	0.10	0.12	0.13	0.12	0.099	0.095
R^2	0.8054	0.8022	0.8133	0.8278	0.8442	0.8345
Intra-particle diffusion						
k_{i1}	7.99	8.46	9.80	9.42	9.32	7.96
R^2	0.9346	0.9668	0.9555	0.9526	0.9838	0.9729
k_{i2}	1.25	1.41	1.64	1.83	1.74	1.50
R^2	0.9209	0.8740	0.8849	0.9266	0.9182	0.9226
k_{i3}	0.18	0.19	0.21	0.23	0.22	0.20
R^2	0.9365	0.9375	0.8589	0.9998	0.8662	0.9999
$q_{e,exp}$	188.13	190.81	196.61	172.85	146.91	126.31

reactions, the experimental data were also assessed using the intra-particle diffusion model, as shown in Fig. 9(d) and Table 1. The intra-particle diffusion curves are not linear over the entire time and could be separated into three linear portions for both adsorbents in the adsorption process. The first stage was the fastest and was attributed to the diffusion of CIP through the bulk solution to the external surfaces of CCFN and ACFN. Moreover, the first stage did not pass through the origin, suggesting that intra-particle diffusion was not the only rate-controlling step, but that this stage was also affected by a multiple layer diffusion process. The second stage corresponded to a gradual adsorption stage. The third stage was the slowest, due to the lower adsorbate concentration, resulting in a lower driving force [34].

The activation energies (E_a) for the adsorption process can be calculated by the Arrhenius equation to be 11.10 and 7.87 kJ/mol for the CCFN and ACFN adsorbents, respectively. Generally, low E_a values (<42 kJ/mol) indicate a diffusion-controlled process [35]. Accordingly, the adsorption behaviors are controlled by a multiple layer diffusion process for CIP adsorption and are evidently physical.

3.6. Adsorption isotherms

The non-linear adsorption isotherms of CIP onto CCFN and ACFN at different temperatures are presented in Fig. 10 and the fitted results are given in Table 2. All isotherms exhibit nonlinear characteristics, and a higher R^2 value implies the applicability of Langmuir and Sips isotherms compared with Freundlich and Temkin isotherms. The Langmuir isotherm is usually used to describe monolayer adsorption. The Sips isotherm is a combined form of the Langmuir and Freundlich expressions deduced for predicting the behavior of heterogeneous adsorption systems [36]. At low adsorbate concentrations, it reduces to the Freundlich isotherm while, at high concentrations, it predicts a monolayer adsorption capacity characteristic of the Langmuir isotherm. The Langmuir and Sips models gave a better fit to the equilibrium adsorption data obtained from the adsorption experiments, indicating that the adsorption of CIP onto CCFN and ACFN occurs via a homogeneous monolayer process. Moreover, the range of R_L values was 0–1, suggesting that CIP adsorption onto the CCFN and ACFN adsorbents was favorable. On the other hand, the higher values

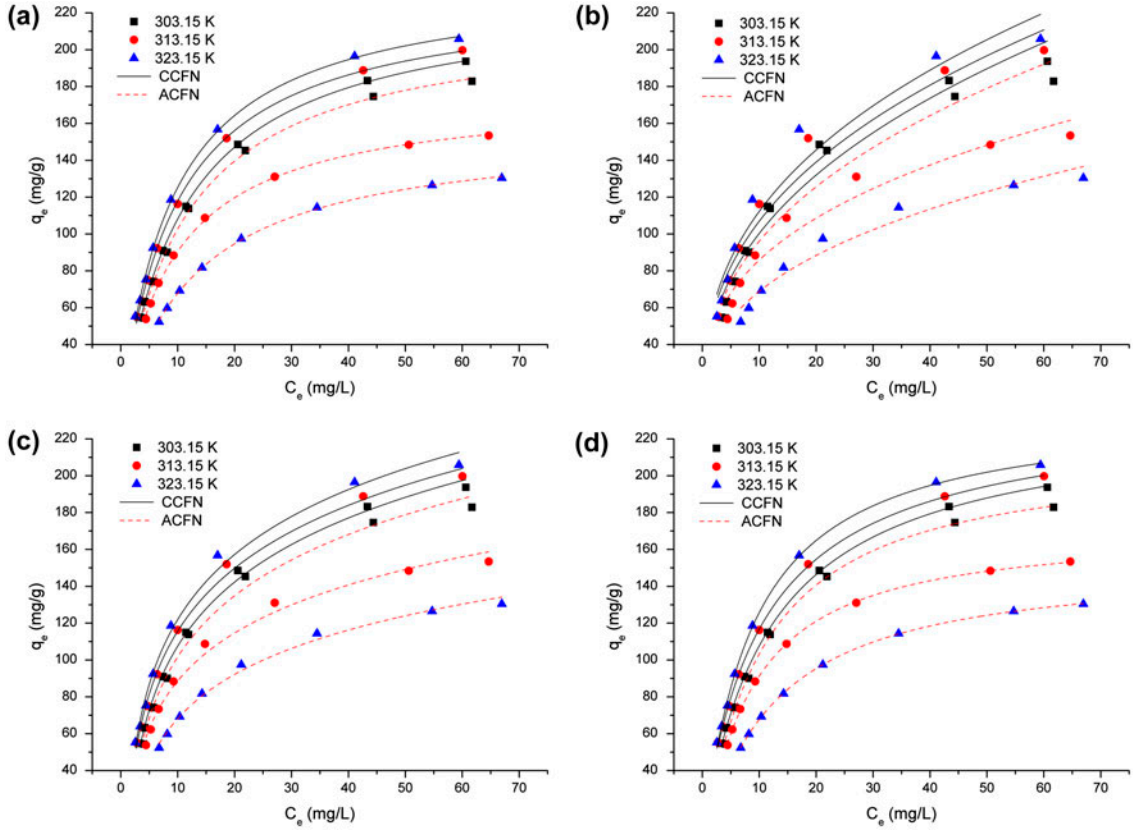

Fig. 10. Adsorption isotherms of CIP on CCFN and ACFN: (a) Langmuir model, (b) Freundlich model, (c) Temkin model and (d) Sips model.

of k_F (40.31, 44.70, 47.27) for CCFN than for ACFN (39.42, 39.30, 30.03) obtained by the Freundlich model also indicated that CCFN has a higher adsorption capacity and affinity for CIP molecules than ACFN. Furthermore, the $1/n_F$ values of the Freundlich isotherm were higher than 1.0 for all temperatures, suggesting that it is favorable for CIP adsorption onto CCFN and ACFN.

The Langmuir maximum adsorption capacities of CIP on CCFN at different temperatures were about 230.02, 230.98, and 238.70 mg/g, which are higher than the corresponding values on ACFN (217.91, 176.63, and 156.96 mg/g). At condition of pH value, CCFN possesses a positive charge in aqueous solution, contributing to the ionic interaction between CCFN and CIP. Therefore, upon cationic modification of CFN a higher adsorption capacity was obtained for CCFN as compared to ACFN (anionic modification) in the present study. Moreover, the comparison of the maximum adsorption capacity (q_{max}) of various adsorbents for CIP is shown in Table 3. The adsorption capacity of CFN has been greatly improved through the modification of the process. The maximum adsorption capacity for CIP on CCFN or ACFN is much higher, indicating that CCFN and ACFN are highly efficient for removing CIP from aqueous solutions.

3.7. Thermodynamic studies

Thermodynamic parameters are presented in Table 4. The positive and negative values of ΔH° indicate that the adsorptions of CIP on CCFN and ACFN are endothermic and exothermic adsorption processes, respectively. The absolute values of ΔG° increased with temperature, implying that higher temperature was favorable for the adsorption of CIP on CCFN, and more the adsorption tendency was opposite on ACFN, which agreed with the ΔH° results. The higher absolute values of ΔG° for the CCFN adsorbent verify the feasibility and spontaneity of the adsorption process with a higher affinity of CIP for CCFN than ACFN [42]. The adsorption process of CIP onto CCFN and ACFN was classified to be a physical process by the absolute values of ΔH° (<40 kJ/mol) [43]. Furthermore, the positive values of ΔS° mean that the adsorption is spontaneous and favorable.

Table 2
Isotherm parameters on the adsorption of CIP onto CCFN and ACFN

	CCFN			ACFN		
Isotherms	303.15 K	313.15 K	323.15 K	303.15 K	313.15 K	323.15 K
Langmuir model						
q_m	230.02	230.98	238.70	217.91	176.63	156.96
K_a	0.089	0.10	0.11	0.11	0.089	0.076
R^2	0.9996	0.9990	0.9989	0.9981	0.9990	0.9996
R_L	0.12	0.11	0.10	0.11	0.12	0.14
Freundlich model						
$1/n_F$	0.40	0.38	0.37	0.39	0.36	0.34
k_F	40.31	44.70	47.27	39.42	39.30	30.03
R^2	0.9632	0.9618	0.9499	0.9521	0.9456	0.9598
Temkin model						
A_T	0.85	1.05	1.10	0.83	1.06	0.71
B	49.25	50.18	50.89	47.94	37.56	34.69
R^2	0.9963	0.9956	0.9819	0.9924	0.9876	0.9921
Sips model						
q_m	234.63	236.36	239.11	211.96	170.40	151.90
K_s	0.092	0.11	0.12	0.094	0.068	0.054
$1/n$	1.02	0.97	0.94	1.05	1.07	1.09
R^2	0.9996	0.9993	0.9987	0.9980	0.9996	0.9999
q_e	183.25	188.79	196.51	174.61	148.38	126.47

Table 3
Comparison of maximum adsorption capacity (q_{max}) of various adsorbents for CIP

Adsorbents	Adsorption isotherm	q_{max} (mg/g)	Refs.
CFN	Langmuir	12.32–15.13	This work
CCFN	Langmuir	230.02–238.70	This work
ACFN	Langmuir	156.96–217.91	This work
Grapheme oxide/calcium alginate	Langmuir	28.59–66.25	[37]
Goethite	Langmuir	33.2–49.9	[38]
Kaolinite	Langmuir	6.3	[11]
Aerobic culture	Langmuir	37.9	[39]
MIP-NIP	Langmuir	11.53	[9]
Carbon xerogel	Langmuir	112	[40]
Carbon nanotubes	Langmuir	135	[40]
Carbon adsorbent from data palm leaflets	Langmuir	104.2–133.3	[41]
Modified coal fly ash	Langmuir	1.443–1.580	[20]

Table 4
Thermodynamic parameters for adsorption of CIP onto CCFN and ACFN

			ΔG° (kJ/mol)		
Adsorbents	ΔH° (kJ/mol)	ΔS° (J/(mol K))	303.15 K	313.15 K	323.15 K
CCFN	9.90	49.09	−4.98	−5.47	−5.97
ACFN	−17.11	47.42	−2.74	−2.25	−1.79

4. Conclusion

In this study, batch adsorption experiments were carried out to investigate the removal of CIP from aqueous solution using cationic and anionic cellulose from FN as adsorbents. The effects of various parameters such as adsorbent dose, contact time, pH, and temperature on the adsorption performance were investigated. The adsorption data fit well with the pseudo-second-order kinetic model and intra-particle diffusion model. The low E_a values of 11.10 (CCFN) and 7.87 kJ/mol (ACFN) indicate the adsorption process is diffusion-controlled. The isotherm adsorption data fit the Langmuir and Sips models well, suggesting that the adsorption of CIP onto CCFN and ACFN occurs via a homogeneous monolayer process. Thermodynamic studies indicated that the adsorption is spontaneous and favorable, and the adsorption of CIP on CCFN is an endothermic process while that on ACFN is an exothermic process.

Acknowledgments

This work was supported by Heilongjiang Province Outstanding Youth Science Fund (JC201301).

References

[1] X.B. Xing, J.W. Feng, G.C. Lv, K.N. Song, L.F. Mei, L.B. Liao, X.Y. Wang, B. Xu, Adsorption mechanism of ciprofloxacin from water by synthesized birnessite, Adv. Mater. Sci. Eng. 2015 (2015) 1–7.
[2] C.-J. Wang, Z. Li, W.-T. Jiang, Adsorption of ciprofloxacin on 2:1 dioctahedral clay minerals, Appl. Clay Sci. 53 (2011) 723–728.
[3] X. Li, S. Chen, X. Fan, X. Quan, F. Tan, Y. Zhang, J. Gao, Adsorption of ciprofloxacin, bisphenol and 2-chlorophenol on electrospun carbon nanofibers: In comparison with powder activated carbon, J. Colloid Interface Sci. 447 (2015) 120–127.
[4] C.G. Daughton, T.A. Ternes, Pharmaceuticals and personal care products in the environment: Agents of subtle change? Environ. Health Perspect. 107 (1999) 907–938.
[5] W.T. Jiang, P.H. Chang, Y.S. Wang, Y. Tsai, J.S. Jean, Z. Li, K. Krukowski, Removal of ciprofloxacin from water by birnessite, J. Hazard. Mater. 250–251 (2013) 362–369.
[6] S. Wu, X. Zhao, Y. Li, C. Zhao, Q. Du, J. Sun, Y. Wang, X. Peng, Y. Xia, Z. Wang, L. Xia, Adsorption of ciprofloxacin onto biocomposite fibers of graphene oxide/calcium alginate, Chem. Eng. J. 230 (2013) 389–395.
[7] M. Khoder, N. Tsapis, H. Huguet, M. Besnard, C. Gueutin, E. Fattal, Removal of ciprofloxacin in simulated digestive media by activated charcoal entrapped within zinc-pectinate beads, Int. J. Pharm. 379 (2009) 251–259.
[8] L. Huang, M. Wang, C. Shi, J. Huang, B. Zhang, Adsorption of tetracycline and ciprofloxacin on activated carbon prepared from lignin with H_3PO_4 activation, Desalin. Water Treat. 52 (2013) 2678–2687.
[9] X.J. Zhang, X.Y. Gao, P.W. Huo, Y.S. Yan, Selective adsorption of micro ciprofloxacin by molecularly imprinted functionalized polymers appended onto ZnS, Environ. Technol. 33 (2012) 2019–2025.
[10] C.J. Wang, Z. Li, W.T. Jiang, J.S. Jean, C.C. Liu, Cation exchange interaction between antibiotic ciprofloxacin and montmorillonite, J. Hazard. Mater. 183 (2010) 309–314.
[11] Z. Li, H. Hong, L. Liao, C.J. Ackley, L.A. Schulz, R.A. MacDonald, A.L. Mihelich, S.M. Emard, A mechanistic study of ciprofloxacin removal by kaolinite, Colloids Surfaces B: Biointerfaces 88 (2011) 339–344.
[12] H. Zhang, C.H. Huang, Adsorption and oxidation of fluoroquinolone antibacterial agents and structurally related amines with goethite, Chemosphere 66 (2007) 1502–1512.
[13] S. Rakshit, D. Sarkar, E.J. Elzinga, P. Punamiya, R. Datta, Mechanisms of ciprofloxacin removal by nano-sized magnetite, J. Hazard. Mater. 246–247 (2013) 221–226.
[14] A. Carlmark, E. Larsson, E. Malmström, Grafting of cellulose by ring-opening polymerisation—A review, Eur. Polym. J. 48 (2012) 1646–1659.
[15] Z.L. Yan, J.C. Zhang, H. Zhang, H. Wang, Improvement of mechanical properties of noil hemp fiber reinforced polypropylene composites by resin modification and fiber treatment, Adv. Mater. Sci. Eng. 2013 (2013) 1–7.
[16] H. Feng, J.A. Li, L.J. Wang, Preparation of biodegradable flax shive cellulose-based superabsorbent polymer under microwave irradiation, Bioresources 5 (2010) 1484–1495.
[17] Q. Ma, L. Wang, Adsorption of Reactive blue 21 onto functionalized cellulose under ultrasonic pretreatment: Kinetic and equilibrium study, J. Taiwan Inst. Chem. Eng. 50 (2015) 229–235.
[18] S.A. Carabineiro, T. Thavorn-Amornsri, M.F. Pereira, J.L. Figueiredo, Adsorption of ciprofloxacin on surface-modified carbon materials, Water Res. 45 (2011) 4583–4591.
[19] K.Y. Foo, B.H. Hameed, Insights into the modeling of adsorption isotherm systems, Chem. Eng. J. 156 (2010) 2–10.
[20] C.-L. Zhang, G.-L. Qiao, F. Zhao, Y. Wang, Thermodynamic and kinetic parameters of ciprofloxacin adsorption onto modified coal fly ash from aqueous solution, J. Mol. Liq. 163 (2011) 53–56.
[21] X. Zhang, J. Tan, X. Wei, L. Wang, Removal of Remazol turquoise Blue G-133 from aqueous solution using modified waste newspaper fiber, Carbohydr. Polym. 92 (2013) 1497–1502.
[22] D.Y. Hu, P. Wang, J. Li, L.J. Wang, Functionalization of microcrystalline cellulose with N,N-dimethyldodecylamine for the removal of congo red dye from an aqueous solution, Bioresources 9 (2014) 5951–5962.
[23] B.-S. Chiou, H. Jafri, T. Cao, G.H. Robertson, K.S. Gregorski, S.H. Imam, G.M. Glenn, W.J. Orts, Modification of wheat gluten with citric acid to produce superabsorbent materials, J. Appl. Polym. Sci. 129 (2013) 3192–3197.

[24] P. Widsten, N. Dooley, R. Parr, J. Capricho, I. Suckling, Citric acid crosslinking of paper products for improved high-humidity performance, Carbohydr. Polym. 101 (2014) 998–1004.
[25] Y.B. Song, Y.X. Sun, X.Z. Zhang, J.P. Zhou, L.N. Zhang, Homogeneous quaternization of cellulose in NaOH/urea aqueous solutions as gene CARRIERS, Biomacromolecules 9 (2008) 2259–2264.
[26] B. Li, Y. Dong, L. Li, Preparation and catalytic performance of Fe(III)-citric acid-modified cotton fiber complex as a novel cellulose fiber-supported heterogeneous photo-Fenton catalyst, Cellulose 22 (2015a) 1295–1309.
[27] X.N. Li, W.Q. Wang, J. Dou, J.S. Gao, S. Chen, X. Quan, H.M. Zhao, Dynamic adsorption of ciprofloxacin on carbon nanofibers: Quantitative measurement by in situ fluorescence, J. Water Process Eng. 9 (2016) e14–e20.
[28] H. Li, D. Zhang, X. Han, B. Xing, Adsorption of antibiotic ciprofloxacin on carbon nanotubes: pH dependence and thermodynamics, Chemosphere 95 (2014) 150–155.
[29] D. Lu, Q. Cao, X. Li, X. Cao, F. Luo, W. Shao, Kinetics and equilibrium of Cu(II) adsorption onto chemically modified orange peel cellulose biosorbents, Hydrometallurgy 95 (2009) 145–152.
[30] H.R. Pouretedal, N. Sadegh, Effective removal of Amoxicillin, Cephalexin, Tetracycline and Penicillin G from aqueous solutions using activated carbon nanoparticles prepared from vine wood, J. Water Process Eng. 1 (2014) 64–73.
[31] S. Zha, Y. Zhou, X. Jin, Z. Chen, The removal of amoxicillin from wastewater using organobentonite, J. Environ. Manage. 129 (2013) 569–576.
[32] J. Febrianto, A.N. Kosasih, J. Sunarso, Y.H. Ju, N. Indraswati, S. Ismadji, Equilibrium and kinetic studies in adsorption of heavy metals using biosorbent: A summary of recent studies, J. Hazard. Mater. 162 (2009) 616–645.
[33] W. Plazinski, W. Rudzinski, A. Plazinska, Theoretical models of sorption kinetics including a surface reaction mechanism: A review, Adv. Colloid Interface Sci. 152 (2009) 2–13.
[34] Y. Sun, Q. Yue, B. Gao, Y. Gao, X. Xu, Q. Li, Y. Wang, Adsorption and cosorption of ciprofloxacin and Ni(II) on activated carbon-mechanism study, J. Taiwan Inst. Chem. Eng. 45 (2014) 681–688.
[35] E.-S.I. El-Shafey, H. Al-Lawati, A.S. Al-Sumri, Ciprofloxacin adsorption from aqueous solution onto chemically prepared carbon from date palm leaflets, J. Environ. Sci. 24 (2012) 1579–1586.
[36] R. Sips, Combined form of langmuir and freundlich equations, J. Chem. Phys. 16 (1948) 490–495.
[37] S.L. Wu, X.D. Zhao, Y.H. Li, C.T. Zhao, Q.J. Du, J.K. Sun, Y.H. Wang, X.J. Peng, Y.Z. Xia, Z.H. Wang, L.H. Xia, Adsorption of ciprofloxacin onto biocomposite fibers of graphene oxide/calcium alginate, Chem. Eng. J. 230 (2013) 389–395.
[38] H. Zhang, C.H. Huang, Adsorption and oxidation of fluoroquinolone antibacterial agents and structurally related amines with goethite, Chemosphere 66 (2007) 1502–1512.
[39] Z.G. Liu, P.Z. Sun, S.G. Pavlostathis, X.F. Zhou, Y.L. Zhang, Adsorption, inhibition, and biotransformation of ciprofloxacin under aerobic conditions, Bioresour. Technol. 144 (2013) 644–651.
[40] S.A.C. Carabineiro, T. Thavorn-amornsri, M.F.R. Pereira, P. Serp, J.L. Figueiredo, Comparison between activated carbon, carbon xerogel and carbon nanotubes for the adsorption of the antibiotic ciprofloxacin, Catal. Today 186 (2012) 29–34.
[41] E.-S.I. El-Shafey, H. Al-Lawati, A.S. Al-Sumri, Ciprofloxacin adsorption from aqueous solution onto chemically prepared carbon from date palm leaflets, J. Environ. Sci. 24 (2012) 1579–1586.
[42] D. Genç, E.C. Dogan, Adsorption kinetics of the antibiotic ciprofloxacin on bentonite, activated carbon, zeolite, and pumice, Desalin. Water Treat. 53 (2013) 785–793.
[43] J.M. Chern, C.Y. Wu, Desorption of dye from activated carbon beds: Effects of temperature, pH and alcohol, Water Res. 35 (2001) 4159–4165.